ANNALS of Clinical and Translational Neurology
Open Access
AMERICAN NEUROLOGICAL ASSOCIATION

RESEARCH ARTICLE

Cardiomyopathy correlates to nerve damage in p.A117S late-onset transthyretin amyloid polyneuropathy

Yen-Hung Lin[1,†], Hsueh-Wen Hsueh[2,†], Mao-Yuan Su[3,†], Mei-Fang Cheng[4,†], Ming-Chang Chiang[5], Jyh-Ming Jimmy Juang[1], Yi-Hui Kao[6], Kai-Chieh Chang[6], Fang-Ping Feng[2], Sung-Tsang Hsieh[2,7,8,9] & Chi-Chao Chao[2]

[1]Department of Internal Medicine, National Taiwan University Hospital, Taipei, Taiwan
[2]Department of Neurology, National Taiwan University Hospital, Taipei, Taiwan
[3]Department of Radiology, National Taiwan University Hospital, Taipei, Taiwan
[4]Department of Nuclear Medicine, National Taiwan University Hospital, Taipei, Taiwan
[5]Department of Biomedical Engineering, National Yang Ming Chiao Tung University, Taipei, Taiwan
[6]Department of Neurology, National Taiwan University Hospital Yunlin Branch, Yunlin, Taiwan
[7]Graduate Institute of Brain and Mind Sciences, National Taiwan University College of Medicine, Taipei, Taiwan
[8]Graduate Institute of Clinical Medicine, National Taiwan University College of Medicine, Taipei, Taiwan
[9]Center of Precision Medicine, National Taiwan University College of Medicine, Taipei, Taiwan

Correspondence
Chi-Chao Chao, Department of Neurology, National Taiwan University Hospital, Taipei, Taiwan. Tel: (886) 2 23123456 ext. 65340; Fax: (886) 2 23418395; E-mail: chichaochao@ntu.edu.tw

Sung-Tsang Hsieh, Department of Anatomy and Cell Biology, National Taiwan University College of Medicine, Taipei, Taiwan. Tel: (886)-2-23123456 ext 88182; Fax: (886)-2-23915292; E-mail: shsieh@ntu.edu.tw

Funding Information
This work was supported by grants from the Ministry of Science and Technology, Taiwan (107-2314-B-002-072-MY2 and 109-2320-B-002-024 to Chi-Chao Chao; 107-2314-B-002-069-MY2, 109-2320-B-002-025, and 110-2320-B-002-072 to Sung-Tsang Hsieh) and the National Taiwan University Hospital (UN109-004 to Chi-Chao Chao and UN109-013 to Sung-Tsang Hsieh).

Received: 8 June 2022; Revised: 30 June 2022; Accepted: 7 July 2022

Annals of Clinical and Translational Neurology **2022; 9(9): 1359–1369**

doi: 10.1002/acn3.51635

†Equal contributions.

Abstract

Objective: Late-onset hereditary transthyretin amyloidosis with polyneuropathy (ATTRv-PN) is often associated with heart involvement. Recent advances in cardiac imaging allow the detection of cardiac amyloidosis. This study aimed to explore cardiomyopathy by cardiac imaging and its clinical correlates with polyneuropathy in late-onset ATTRv-PN. **Methods**: Polyneuropathy was assessed by intraepidermal nerve fiber (IENF) density, nerve conduction study (NCS), autonomic function tests, quantitative sensory testing, and clinical questionnaires. Cardiomyopathy was evaluated by echocardiography, ^{99m}Tc-pyrophosphate (PYP) single-photon emission computed tomography (SPECT) imaging, cardiac magnetic resonance imaging (CMR), and serum Pro-B-type natriuretic peptide. Healthy controls and patients with Brugada syndrome were enrolled for comparison of CMR. **Results**: Fifty late-onset ATTRv-PN patients (38 men, 46 with p.A117S mutation), aged 63.7 ± 5.5 years, of polyneuropathy disability stage 1–4 were enrolled. All patients presented polyneuropathy in NCS, and 74.5% of patients had reduced IENF density in distal legs. All patients showed significant radiotracer uptake in the heart on ^{99m}Tc-PYP SPECT imaging, and 87.8% of patients had abnormally increased left ventricular (LV) septum thickness on echocardiography. CMR showed longer myocardial native T1, larger extracellular volume, greater LV mass index, and higher LV mass to end-diastolic volume ratio in ATTRv-PN patients than healthy controls and patients with Brugada syndrome. These CMR parameters were associated with skin denervation, absent sympathetic skin responses, elevated thermal thresholds, worsened NCS profiles, and functional deficits of polyneuropathy. **Interpretation**: Late-onset ATTRv-PN coexisted with cardiomyopathy regardless of the clinical severity of polyneuropathy. The cardiac amyloid burden revealed by CMR was correlated with pathophysiology and clinical disability of nerve degeneration.

Introduction

Hereditary transthyretin (TTRv) amyloidosis (ATTRv) is a systemic disease caused by TTR gene mutation. The amino acid changes of TTR lead to protein misfolding and formation and extracellular deposition of amyloid in various tissues throughout the body.[1] Patients with ATTRv exhibit variable clinical phenotypes depending on the sites of amyloid deposition, and the peripheral nervous system is the most commonly involved organ, followed by the heart.[2] The cardinal feature of ATTRv with polyneuropathy (ATTRv-PN) is adult-onset, length-dependent neuropathy presenting with motor weakness, sensory impairment and paraesthesia, and pandysautonomia affecting sympathetic, parasympathetic, and enteric functions. All patients follow a progressive course, and most patients become disabled within years.[3] Although neuropathy progresses relentlessly and is the dominant manifestation in ATTRv-PN, the presence of cardiomyopathy is the main prognostic determinant, and survival is shorter in ATTRv-PN patients with cardiac involvement than in those presenting with only polyneuropathy.[4,5] These observations indicated that integrated care for both polyneuropathy and cardiomyopathy and tight cooperation between neurologists and cardiologists are critical for a better prognosis of ATTRv-PN.[6] However, the relationship between polyneuropathy and cardiomyopathy in ATTRv-PN has not been elucidated, and there is a lack of neuropathic parameters that can reflect or predict the progression of cardiomyopathy.

Previous literature has shown that cardiomyopathy in ATTRv-PN is usually underdiagnosed,[7] and the clinical manifestation of cardiomyopathy, such as fatigue, exertional dyspnea, exercise intolerance, or peripheral edema, could be masked by concomitant polyneuropathy. Recent developments in imaging technology, including repurposed bone scintigraphy and cardiac magnetic resonance (CMR) imaging, have improved the detection of cardiomyopathy in the absence of tissue biopsy.[8] CMR can provide accurate and detailed information about the changes in cardiac tissue and morphology by demonstrating late gadolinium enhancement and measuring the myocardial T1 time, extracellular volume (ECV), and left ventricular mass index (LVMi).[9] Bone-avid radiotracers, such as technetium-99m (^{99m}Tc)-pyrophosphate (PYP), have been recognized as semiquantitative tools in diagnosing cardiac amyloidosis in ATTRv.[10,11] After excluding light-chain amyloidosis, the ^{99m}Tc PYP scan can identify TTR-related cardiomyopathy with high sensitivity and specificity and can be a potential prognostic factor.[12] These advances in diagnostic imaging have allowed early detection of cardiac involvement and might alter the therapeutic strategy in ATTRv-PN. However, their performance in late-onset ATTRv-PN with cardiomyopathy and their associations with the progression of polyneuropathy have not been clarified.

In contrast to the most common TTR p. V50M mutation in western countries and Japan,[13] p. A117S mutation constitutes the majority of late-onset ATTRv-PN with cardiomyopathy in Taiwan and has also been reported in China and Southeast Asia.[14–17] Our recent report comparing the manifestations in patients with p. A117S and late-onset p. V50M showed comparable clinical phenotypes and disease progression, and heart failure or sudden death due to cardiac amyloidosis was the predominant cause of death in both groups of patients.[18] In the present study, we combined echocardiography, CMR, and ^{99m}Tc PYP scans to explore cardiac involvement in late-onset ATTRv-PN with predominant p. A117S genotype, which is invariantly associated with cardiomyopathy during the disease course.[18,19] We aimed to explore the phenotypes of cardiac amyloidosis and their correlates with the clinical manifestation of polyneuropathy in late-onset ATTRv-PN.

Materials and Methods

Subjects

The study enrolled patients with ATTRv-PN. The inclusion criteria included (1) transthyretin pathogenic mutation, (2) clinical evidence of sensorimotor or autonomic neuropathic symptoms and neuropathological evidence of axonal polyneuropathy on skin biopsy or nerve conduction studies, and (3) no monoclonal paraprotein in the serum by immunoelectrophoresis. Patients with alternative causes of polyneuropathy, including diabetes mellitus, renal insufficiency, autoimmune disorders, infections, toxin exposure, nutrition insufficiency, or malignancy, were excluded. This study was approved by the Ethics Committee of the National Taiwan University Hospital. Written informed consent was obtained from all participants before all procedures in the study.

All participants received clinical evaluations, including the assessment of clinical symptoms, neurological examinations, and questionnaires. Disability was evaluated according to the polyneuropathy disability (PND) staging system, including stage 1, sensory symptoms without motor disturbances; stage 2, minor motor disturbances and ability to walk without aids; grade 3, major motor disturbances and requiring unilateral (3a) or bilateral (3b) support to walk; and grade 4, confinement to a bed or a wheelchair. The questionnaires included World Health Organization Quality of Life Instruments (WHOQOL-BREF) to assess life quality, the Rasch-built Overall Disability Scale (R-ODS) to capture activity and social participation limitations, and a survey of autonomic symptoms (SAS) to evaluate autonomic dysfunction. Laboratory tests included nerve

conduction studies (NCS), quantitative sensory testing, autonomic function tests, and skin biopsies with quantitation of epidermal innervation for evaluation of neuropathy and cardiac echo, ^{99m}Tc-PYP single-photon emission computed tomography (SPECT) imaging, cardiac magnetic resonance imaging, and serologic pro-B-type natriuretic peptide (pro-BNP) for evaluation of cardiomyopathy. All the above examinations were performed in the National Taiwan University Hospital.

Skin biopsy and quantitation of skin epidermal innervation

A 3-mm-diameter skin punch was taken from the distal lateral leg 10 cm proximal to the lateral malleolus under local anesthesia with 2% lidocaine. Fifty micrometers perpendicular to the dermis were immunostained with antiserum to protein gene product 9.5 (PGP 9.5, 1: 1000; UltraClone, Isle of Wight, UK), and the reaction product was demonstrated using chromogen SG (Vector Laboratories). PGP 9.5-immunoreactive epidermal nerve fibers were quantified through the depth of the entire section by examiners blinded to the clinical information following an established protocol.[20] The length of the epidermis along the upper margin of the stratum corneum in each skin section was measured with NIH ImageJ vers. 1.43 (http://rsbweb.nih.gov/ij/download.html, Bethesda, MD). Intraepidermal nerve fiber (IENF) density was expressed as the number of fibers/mm of epidermal length. In the distal leg, normative values from our laboratory (mean ± SD, 5th percentile) of IENF were 11.16 ± 3.70 and 5.88 fibers/mm for subjects aged <60 years and 7.64 ± 3.08 and 2.50 fibers/mm for subjects aged ≥60 years.

Nerve conduction study

A nerve conduction study (NCS, Nicolet Viking, Madison, WI) was performed following established methods in a temperature-controlled room.[21,22] The median and ulnar nerves of the upper limbs and the peroneal, tibial, and sural nerves of the lower limbs were studied. A sensory nerve conduction study was performed antidromically. Abnormal results in NCS were defined as having reduced amplitude of compound muscle action potential (CMAP) or sensory nerve action potential (SNAP), prolonged distal latency, or slowing of the nerve conduction velocity according to the normative data of our laboratory.[22] For the NCS sum score, we calculated the number of standard deviations from the mean (Z score) based on the reference values in our laboratory in five NCS parameters, including distal ulnar CMAP, distal peroneal CMAP, distal tibial CMAP, ulnar SNAP, and sural SNAP.[23] The NCS sum score was the summation of the Z scores from these five NCS parameters.

Quantitative sensory testing

Sensory thresholds were assessed using a Thermal and Vibratory Sensory Analyzer (Medoc Advanced Medical System, Minneapolis, MN) as described previously.[24] Thermal thresholds were recorded at the thenar eminence and foot dorsum according to the algorithm of levels and were expressed as the warm and cold threshold temperatures. Vibratory thresholds were measured at the lateral malleolar process with similar algorithms and were expressed in micrometers. These values were compared with the normative values for age according to our previous report.[24]

Autonomic function tests

Sympathetic skin response (SSR) for sudomotor function and R–R interval variability (RRIV) for cardiac-vagal function were performed using established protocols on the Nicolet Viking IV Electromyographer (Madison, WI).[25] The SSR was recorded from the palm and sole, and the results were interpreted as the presence or the absence without quantitation of latencies and amplitude because of their significant variations. The RRIV was obtained at rest and during deep breathing. Each test was repeated three times, and the mean value was compared with that of the age-matched controls in our laboratory.

Cardiac magnetic resonance imaging and image analysis

Cardiac magnetic resonance imaging (CMR) was performed on a 1.5-T Magnetom Aera (Siemens Healthcare, Erlangen, Germany) with a 30-channel cardiac coil array. Myocardial T1 mapping was performed with electrocardiography (ECG)-triggered modified Look-Locker inversion recovery (MOLLI) pulse sequence before and 10 min after 0.15 mmol/kg intravenous administration of the gadolinium-based contrast agent (Dotarem, Guerbet, France). The scan parameters were as follows: TE/TR 1.14/2.7 msec, flip angle 35°, bandwidth 977 Hz/Px, minimum TI 125–150 msec, TI increment 80 msec, pixel spacing 1.36 × 1.36 mm^2, and slice thickness 8 mm. Cine MRI was performed using a segmented balanced steady-state gradient-echo pulse sequence with a retrospective ECG R-wave trigger. Scan parameters were as follows: TE/TR 1.6/3.0 msec, flip angle 50–70°, bandwidth 975 Hz/Px, pixel spacing 1.25 × 1.25 mm^2, slice thickness 8 mm, and gap 2 mm. A total of 10–12 short axis slices were obtained, depending on cardiac size. Thirty cardiac phases were acquired for each level. After postcontrast T1 acquisition, LGE images were acquired using an ECG-triggered phase-sensitive inversion recovery prepared segmented fast gradient-echo pulse sequence to identify focal fibrosis or scarring.

Commercial postprocessing software (cvi42, Circle Cardiovascular Imaging, Calgary, AB, Canada) was used to measure the myocardial native T1, extracellular volume fraction (ECV), LVMi, and mass-to-volume ratio (MVR) offline. The myocardial native T1 and ECV were calculated from pre- and postcontrast T1 maps using a region-based method.[26] The ROIs in the blood and myocardium of the left ventricle were drawn in the central area of the LV cavity and the septal myocardium on the T1-mapping image at the middle slice. If the septal myocardium showed regional hyperenhancement on the LGE images, the regions of interest of the myocardium were redrawn in other unenhanced myocardial regions. The average T1 values of the segmented regions of interest were then computed. After subtracting the precontrast values from the postcontrast values, the changes in the relaxation rate (1/T1) in the blood and the myocardium were obtained. Myocardial ECV values were calculated by using the ratio of the change in relaxation rate in the myocardium to that in the blood and multiplied by (1-hematocrit). Imaging analysis for LVMi was performed in accordance with the guidelines from the society for cardiovascular magnetic resonance.[27–29] After obtaining the end-diastolic volume (EDV) and end-systolic volume (ESV) of the LV, the LV mass was computed by the difference in LV epicardial volume between EDV and ESV, multiplied by the density of the myocardium, 1.05 g/mL. LVMi was calculated from LV mass divided by body surface area. The LV geometric remodeling was determined from the mass-to-volume ratio (MVR) by calculating the ratio of LV mass with respect to LV EDV.

^{99m}Tc-PYP SPECT imaging

Planar and SPECT imaging of the chest was performed at 3 h after intravenous injection of 20 mCi of technetium pyrophosphate (^{99m}Tc-PYP).[30] The image acquisition parameters and protocol followed the joint guidelines established by the Taiwan Society of Cardiology and the Society of Nuclear Medicine of the Republic of China[11] and the multisocietal expert consensus recommendation.[27,31] The images were analyzed visually and semiquantitatively by visual score and the heart-to-lung contralateral ratio (H/CL ratio), respectively. A visual score of tracer uptake in the left ventricular (LV) myocardium is given as follows: grade 0: no uptake, grade 1: uptake less than a rib, grade 2: uptake equal to that of rib, and grade 3: uptake greater than rib.[11] A positive scan was defined as a visual score ≥grade 2, which is strongly suggestive of ATTR-CM.

Echocardiography

An echocardiographic ultrasound system (IE33, Philips; Andover, MA) was applied to perform echocardiography. Echocardiographic studies, including two-dimensional, M-mode and Doppler ultrasound recordings, were performed. Interventricular septum thickness in diastole (IVSd), LV posterior wall thickness in diastole, and LVEF were measured according to the procedures of the American Society of Echocardiography.[32] The normal references of the echocardiographic parameters were based on a previous report from the same populations.[33]

Data analysis

Numerical variables were expressed as the mean ± SD and were compared with *t* tests if the data followed a Gaussian distribution or nonparametric tests if not. Fisher's exact test was used to compare categorical data. Correlations between variables were analyzed by simple linear regression and multiple linear regression models with the covariance of Model R^2 and standardized correlation coefficients. Age and sex were corrected in all analyses. Multiple comparisons across the regression tests were corrected using the false discovery rate (FDR) method with the FDR of the regression tests controlled at 5%.[34] All analyses were performed using Stata software (StataCorp LP, College Station, TX) and GraphPad Prism (GraphPad Software, San Diego, CA). The results were considered significant at $p < 0.05$.

Results

Clinical manifestations

We recruited 50 patients (38 men) with ATTRv-PN aged 63.7 ± 5.5 years (53–77 years). The duration from the onset of neuropathic symptoms was 3.7 ± 2.2 years (0.3–9 years). Based on neurological deficits, 6 patients were in PND stage 1 with only sensory or autonomic symptoms, 13 patients were in PND stage 2, 15 patients were in PND stage 3a requiring unilateral walking assistance, 5 patients were in PND stage 3b using bilateral walking support, and 11 patients were in PND stage 4 and wheelchair dependent. The genotype of these patients included p. A117S mutation (46 cases), p. E109K (2 cases), p. F53L (1 case), and p. V50M (1 case). For the limitations during physical activity defined by the New York Heart Association (NYHA) classification, 11 of the patients were in NYHA class I, 38 were in class II, and 1 was in class III. The total raw scores of the R-ODS, WHOQOL-BREF, and SAS were 29.6 ± 14.5 (range 2–48), 92.5 ± 10.1 (range 68–105), and 13.2 ± 7.9 (range 0–35), respectively.

Neurophysiology, neuropathology, and psychophysics

Table 1 shows the data of intraepidermal nerve fiber density on skin biopsy, nerve conduction study, SSR, RRIV,

Table 1. Skin innervation, neurophysiology, and psychophysics in patients with hereditary transthyretin amyloidosis with polyneuropathy and cardiomyopathy (ATTRv-PN).

	ATTRv-PN patients	Normal references
Skin biopsy	47 cases	
IENF density (fibers/mm)	2.02 ± 1.93	>5.88, for age < 60 years
Abnormal IENF density	74.5%	>2.50, for age ≥ 60 years
NCS (value and abnormal rate)	50 cases	
Median nerve		
Distal motor latency (msec)	6.2 ± 1.7 (94%)	≦4.2
Distal CMAP (mV)	2.4 ± 2.0 (84%)	≧4.6
Motor conduction velocity (m/s)	44.7 ± 6.0 (84%)	≧50
Distal SNAP (μV)	3.2 ± 5.1 (84%)	≧10
Sensory conduction velocity (m/s)	42.7 ± 6.1 (96%)	≧50
Ulnar nerve		
Distal motor latency (msec)	3.8 ± 0.8 (56%)	≦3.5
Distal CMAP (mV)	4.5 ± 2.9 (64%)	≧6.0
Motor conduction velocity (m/s)	47.1 ± 6.1 (48%)	≧50
Distal SNAP (μV)	5.9 ± 6.3 (78%)	≧8
Sensory conduction velocity (m/s)	50.1 ± 5.4 (56%)	≧50
Peroneal nerve		
Distal motor latency (msec)	5.1 ± 1.3 (58%)	≦5.5
Distal CMAP (mV)	1.0 ± 1.5 (80%)	≧2.0
Motor conduction velocity (m/s)	39.1 ± 5.5 (76%)	≧40
Tibial nerve		
Distal motor latency (msec)	4.6 ± 1.2 (42%)	≦5.5
Distal CMAP (mV)	1.8 ± 2.6 (90%)	≧6.0
Motor conduction velocity (m/s)	38.9 ± 4.5 (70%)	≧40
Sural nerve		
Distal SNAP (μV)	1.5 ± 2.7 (92%)	≧5.0
Sensory conduction velocity	42.8 ± 3.8 (76%)	≧40
NCS Z score		
Ulnar CMAP Z score	2.78 ± 1.54	NA
Peroneal CMAP Z score	2.27 ± 0.85	NA
Tibial CMAP Z score	2.87 ± 0.68	NA
Ulnar SNAP Z score	2.22 ± 0.51	NA
Sural SNAP Z score	2.82 ± 0.60	NA
NCS sum score	12.96 ± 3.62	NA
Sympathetic skin response, *n* (%)	48 cases	
Absence at palms	18 (37.8%)	Presence
Absence at soles	33 (68.8%)	Presence
R–R interval variability (%)		Age/at rest/deep breathing
At rest (33 cases)	4.1 ± 2.2 (91%)	20–29 y/o/12–46%/19–62%
During deep breathing (24 cases)	5.3 ± 2.4 (88%)	30–39 y/o/6–32%/9–54%
		40–49 y/o/6–36%/14–48%
		50–59 y/o/5–23%/11–39%
		60–69 y/o/7–19%/8–28%
Sensory thresholds	47 cases	For age < 40, 40 to < 60, ≧60 y/o
Warm at thenar (°C)	38.0 ± 6.1 (70.2%)	≦34.3, ≦34.6, ≦34.9
Cold at thenar (°C)	25.5 ± 9.4 (65.9%)	≧29.9, ≧29.6, ≧29.4
Warm at foot dorsum (°C)	44.2 ± 4.9 (63.8%)	≦38.6, ≦40.1, ≦40.6
Cold at foot dorsum (°C)	20.6 ± 11.5 (44.7%)	≧27.5, ≧26.7, ≧27.0
Vibratory at ankle	56.7 ± 50.9 (75.6%)	≦4.0, ≦7.0, ≦10.0

CMAP, compound muscle action potential; IENF, intraepidermal nerve fiber; NA, not applicable; NCS, nerve conduction study; *n*, number of cases; MNE, median nerve entrapment; SNAP, sensory nerve action potential; y/o, years old.

and quantitative sensory test. All patients showed polyneuropathy in the nerve conduction study, and the NCS sum score was 12.96 ± 3.62 (range 3.95–17.50). The IENF density was 2.02 ± 1.93 fibers/mm, and approximately three-fourths (74.5%) of patients had abnormally reduced IENF density. A total of 68.8% and 37.8% of

patients had absent sympathetic skin responses at the soles and palms, and 90.9% and 87.5% of patients had reduced R–R interval variability at rest and during deep breathing. For quantitative sensory testing, 44.7%–70.2% had abnormally elevated thermal thresholds at the hands and feet, and 75.6% of patients had increased vibratory thresholds at the ankle.

^{99m}Tc-PYP SPECT imaging, echocardiography, and pro-B-type natriuretic peptide

Forty-nine patients received ^{99m}Tc-PYP SPECT imaging, and all showed significant radiotracer uptake in the heart. The visual score was grade 2 in 21 patients (42.9%) and grade 3 in 28 patients (57.1%). The H/CL ratio was 1.61 ± 0.17. In echocardiographic measurements (n = 49), the IVSd was 14.8 ± 3.2 mm, the LV posterior wall thickness in diastole was 14.0 ± 2.6 mm, and the left ventricular ejection fraction (LVEF) was 61.7% ± 11.1%. Compared with the normal references based on the healthy population, the patients with more than 2 standard deviations from the mean were 87.8% in IVSd and 28.6% in LVEF. The pro-BNP was 2358.4 ± 4923.1 pg/mL, 91.7% of patients had pro-BNP higher than the normal reference value (125 pg/mL), and 45.8% of patients had pro-BNP higher than the cutoff value for heart failure (900 pg/mL).

Cardiac magnetic resonance imaging

In the cardiac magnetic resonance (CMR) study (n = 50), 35 (70%) patients showed ventricular hypertrophy, including LV hypertrophy in only 31 patients and bilateral ventricular hypertrophy in 4 patients. Twenty-seven patients (54%) showed hypokinesia or akinesia of the LV. Forty patients had subendocardial delayed enhancement in the LV myocardium (7 cases) or biventricular myocardium (33 cases). Myocardial native T1 and ECV values, the primary measurement of myocardial amyloidosis burden, were 1138.5 ± 53.2 msec (range 1021.0–1275.2) and 46.4% ± 8.7% (range 32.5–68.7), respectively. The LVMi was 103.7 ± 35.9 g/m^2 (range 54.6–185.9), and the ratio of LV mass to LV EDV (MVR) was 1.77 ± 0.67 (range 0.68–3.84).

For comparison of cardiac MRI with ATTRv-PN patients, we enrolled 36 normal healthy controls (12 men), aged 30.0 ± 12.3 years (21–58 years), and 27 patients with Brugada syndrome (22 men), aged 62.1 ± 8.3 years (51–78 years). The latter was an inherited cardiac disease leading to ventricular arrhythmia in structurally normal hearts and was selected as disease control. ATTRv-PN patients had more male cases and were older than healthy controls (both $p < 0.001$), and there were no significant differences in the sex or age between patients with ATTRv-PN and Brugada syndrome. (p = 0.586 and 0.296, respectively). Figure 1 shows the myocardial native T1 and extracellular volume from the representative cases of healthy control, Brugada syndrome, and ATTRv-PN. The myocardial native T1 was longer and the extracellular volume was larger in the ATTRv-PN patient than in both the healthy control and the patient with Brugada syndrome. Further analysis comparing to healthy controls and patients with Brugada syndrome with correction of age and gender factors showed that ATTRv-PN patients had significantly longer myocardial native T1 (1138.5 ± 53.2 vs. 1005.3 ± 28.6 and 1019.4 ± 23.8 msec, both $p < 0.001$; Fig. 2A), larger ECV (46.4 ± 8.7 vs. 23.7 ± 2.3 and 25.4% ± 1.2%, both $p < 0.001$; Fig. 2B), higher LVMi (103.7 ± 35.9 vs. 53.0 ± 11.4 and 54.2 ± 9.9 g/m^2, both $p < 0.001$; Fig. 2C), and higher MVR (1.77 ± 0.67 vs. 0.81 ± 0.11 and 0.99 ± 0.27, both $p < 0.001$; Fig. 2D).

Correlation of cardiomyopathy and polyneuropathy

We further investigated whether the parameters of cardiomyopathy could reflect the clinical severity and functional deficits of late-onset ATTRv-PN (Table 2). The cardiomyopathic parameters included the visual score and H/CL ratio of ^{99m}Tc-PYP SPECT, IVSd, and LVEF on echocardiography, ECV, myocardial native T1, LVMi and MVR on CMR, and pro-BNP blood level. With age and sex as covariants in the multiple linear regression model, we found that CMR and pro-BNP were best correlated with PND stage, WHOQOL_BREF, R-ODS, and SAS, including (1) higher MVR correlated with higher PND stage, (2) higher ECV, higher LVMi, and higher pro-BNP levels were associated with lower quality of life, as shown by WHOQOL_BREF raw scores, (3) longer myocardial native T1, higher LVMi and MVR correlated with lower functional status measured by R-ODS raw scores, and (4) higher ECV was associated with increased autonomic dysfunction demonstrated by SAS.

We then explored the association between cardiomyopathy and polyneuropathy in these patients with late-onset ATTRv-PN, and the neuropathic parameters included IENF density and thermal thresholds at the foot dorsum for small-fiber sensory nerves, SSR at the palm and sole for autonomic function, and NCS sum scores for large-fiber sensory and motor nerves. Using a multiple regression model with age and sex as covariants, the results showed that (1) higher ECV on CMR was associated with lower IENF density on skin biopsy, (2) higher LVMi and MVR were associated with the absence of SSR at the soles and/or palms, (3) lower cold threshold temperature at the foot dorsum, and (4) higher MVR

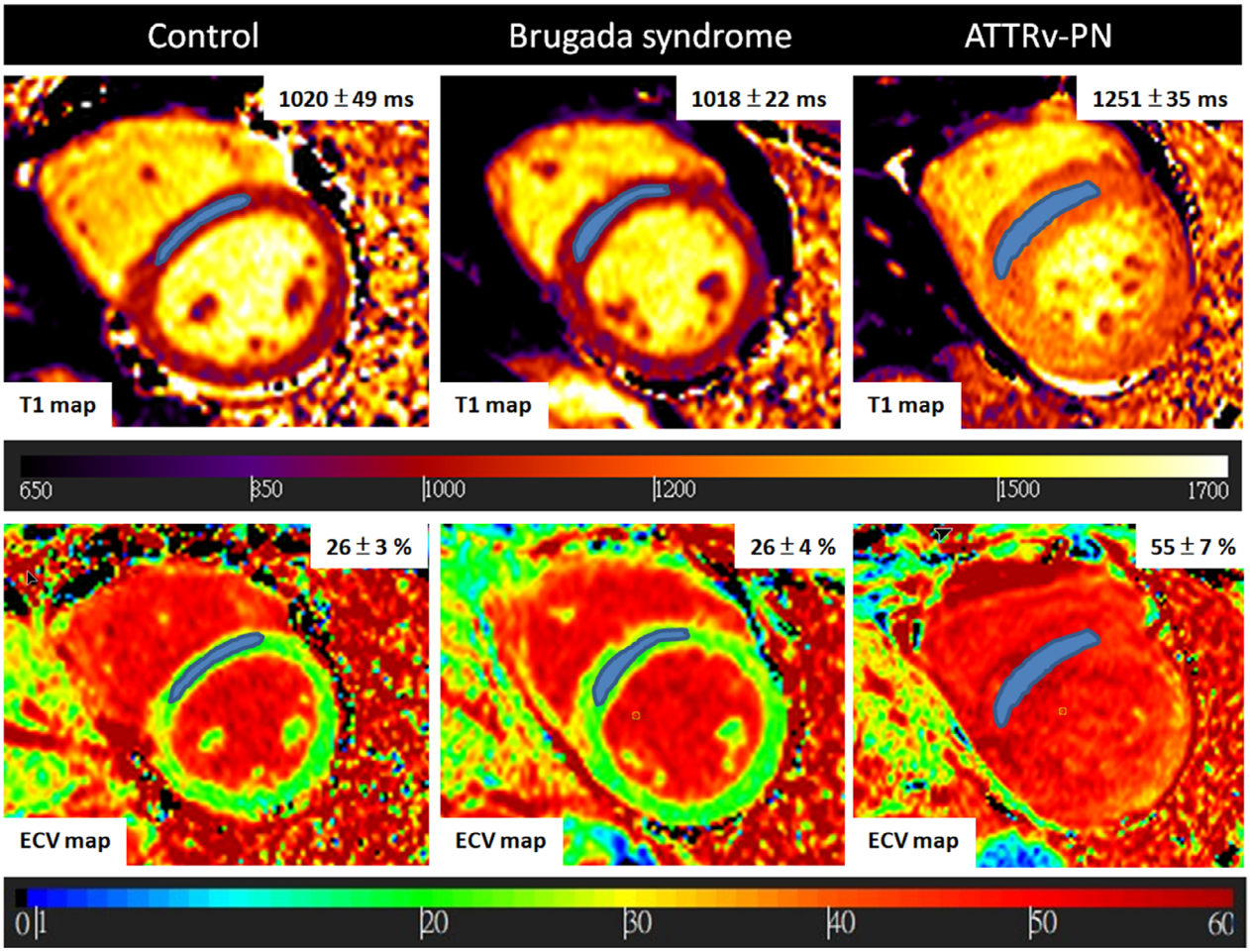

Figure 1. Myocardial native T1 and extracellular volume measurements on cardiac magnetic resonance imaging in a control subject and age- and gender-matched representative patients with Brugada syndrome and hereditary transthyretin amyloidosis with polyneuropathy (ATTRv-PN). The regions of interest were drawn in the middle septum of the left ventricle on the myocardial native T1 (top row, msec) and extracellular volume (bottom row, %) maps. The myocardial native T1 and extracellular volume of the ATTRv-PN patient were much longer and larger than those of the healthy subject and the patient with Brugada syndrome.

correlated with higher NCS sum scores. ^{99m}Tc-PYP SPECT was not associated with clinical severity, functional deficits, or neuropathic parameters.

Discussion

The present study investigated the cardiomyopathic changes and their clinical and neuropathic associations in late-onset ATTRv-PN patients, the majority of whom were p. A117S mutant, which shared a similar phenotype to p. V50M mutant.[18] The important findings included (1) all the enrolled late-onset ATTRv-PN patients with various stages of severity consistently manifested cardiomyopathy as shown by significant radiotracer uptake on ^{99m}Tc-PYP SPECT imaging, (2) the cardiomyopathy was associated with compromised cardiac functional capacity (NYHA class I–III), significantly thicker IVSd on echocardiography; higher ECV, longer myocardial native T1, increased LVMi, and higher MVR on CMR, and elevated pro-BNP in the blood, (3) the abnormal CMR parameters and elevated pro-BNP level were associated with higher clinical stage, lower quality of life, more severe disability, and more autonomic dysfunction, and (4) there were significant correlations between the CMR biomarkers of cardiomyopathy and pathophysiological parameters of polyneuropathy. These findings suggested that cardiomyopathy is highly prevalent, related to neuropathic changes in both small- and larger-fiber nerves and can reflect the overall severity and functional deficits in late late-onset ATTRv-PN patients.

ATTRv-PN is a lethal, gain-of-toxic-function disorder characterized by extracellular deposition of TTR-

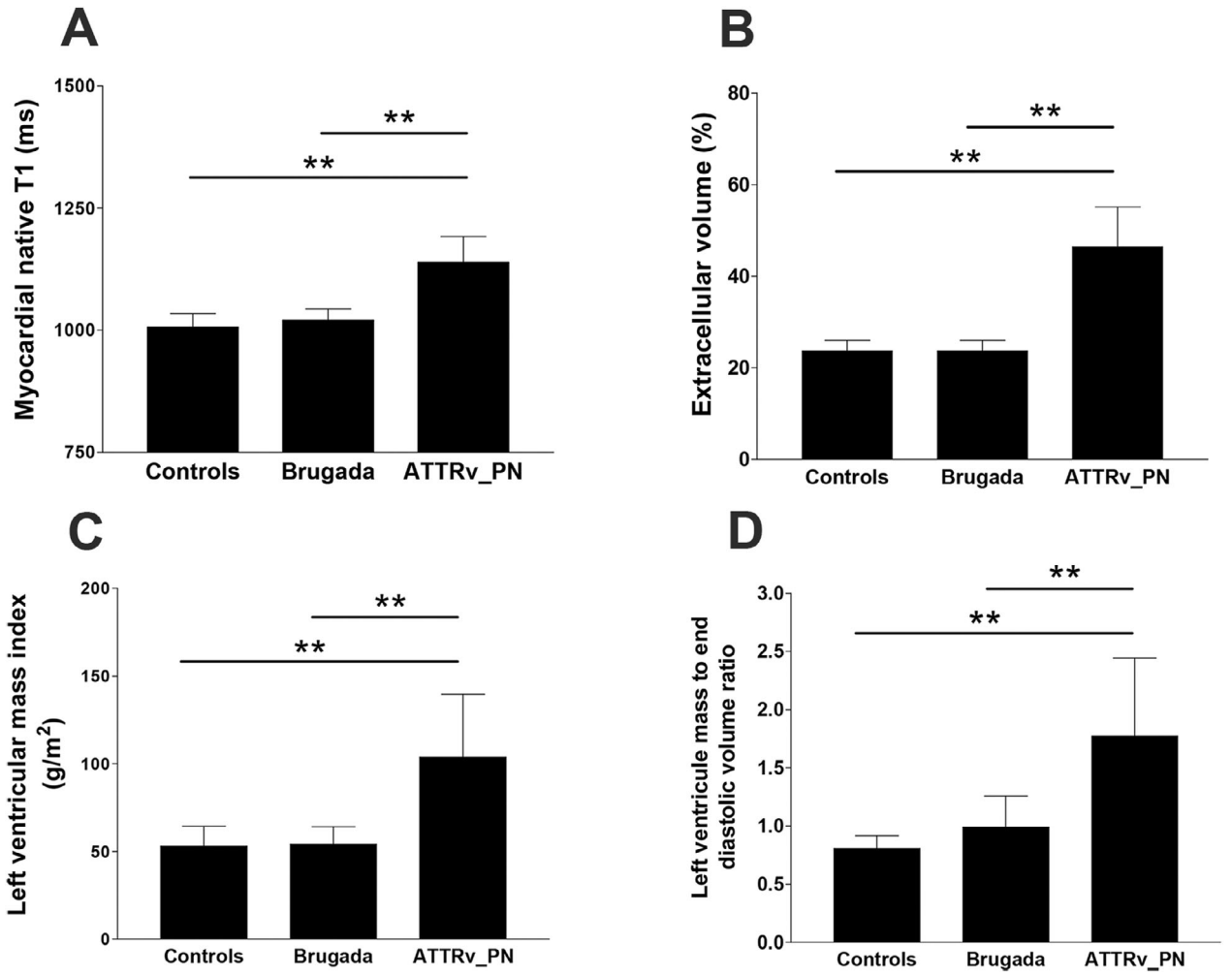

Figure 2. Comparison of cardiac magnetic resonance imaging among healthy controls and patients with Brugada syndrome and hereditary transthyretin amyloidosis with polyneuropathy (ATTRv-PN). (A) The myocardial native T1 was significantly longer, (B) the extracellular volume was much larger, (C) the left ventricular mass index was remarkably greater, and (D) the left ventricular mass to end-diastolic volume ratio was markedly higher in patients with ATTRv-PN than in healthy controls and patients with Brugada syndrome. $^{**}p < 0.001$.

containing amyloid fibrils predominantly in the peripheral nerves. There are over 130 pathogenic mutations of the TTR gene, and there is an association between the specific mutation and the predominant phenotype, although there is considerable overlap.[1,3] Although the heart is also commonly involved in ATTRv-PN,[35] especially in the late-onset form,[4,18] the cardiac manifestations, and their clinical associations with polyneuropathy in ATTRv-PN, are not clear. In the present study, all the enrolled patients with late-onset ATTRv-PN with different severities from the early to late PND stage consistently showed remarkable ^{99m}Tc-PYP uptake, and all visual scores were equal to or larger than grade 2. The bone-avid radiotracer ^{99m}Tc-PYP has been proven to be a noninvasive tool in detecting cardiac amyloidosis and has very high sensitivity and specificity in diagnosing cardiac amyloidosis caused by TTR protein after excluding the presence of monoclonal paraprotein.[30,36] In our late-onset ATTRv-PN patients, all had confirmed TTR mutations with a clear neuropathic phenotype and no monoclonal paraprotein in the blood; therefore, the abnormal uptake in ^{99m}Tc-PYP SPECT imaging must have resulted from TTRv cardiomyopathy. The significantly increased ^{99m}Tc-PYP radiotracer uptake (visual score ≥ 2) noted even in those PND 1 patients suggested that the cardiomyopathy not only coexisted with polyneuropathy but also probably preceded the development of clinical polyneuropathy.

In addition to ^{99m}Tc-labeled bone-avid scintigraphy, the cardiomyopathy in our patients with late-onset ATTRv-PN was associated with significant changes in echocardiography, CMR, and serological biomarkers. On echocardiography, cardiac amyloidosis was characterized by an increased

Table 2. The correlation between the imaging and serologic biomarkers of cardiomyopathy and the pathophysiology and functional disability of polyneuropathy.

	^{99m}Tc-PYP SPECT		Cardiac echo		Cardiac MRI				
	PYP score	H/CL ratio	IVSd	LVEF	ECV	Myo T1	LVMi	MVR	Pro-BNP
PND stage	−0.010, 0.904	0.003, 0.929	0.022, 0.647	−1.088, 0.550	2.240, 0.122	19.252, 0.025	11.651, 0.039	0.305, 0.004*	994.989, 0.231
WHOQOL_BREF	−0.004, 0.598	−0.001, 0.690	−0.008, 0.070	0.434, 0.012	−0.450, 0.001*	−1.560, 0.071	−1.462, 0.005*	−0.022, 0.024	−272.905, <0.001*
R-ODS	−0.003, 0.603	−0.001, 0.926	−0.002, 0.454	0.220, 0.074	−0.214, 0.030	−1.675, 0.004*	−0.980, 0.006*	−0.018, 0.008*	−95.496, 0.098
SAS	−0.001, 0.984	0.003, 0.445	0.010, 0.071	−0.394, 0.079	0.556, 0.001*	2.174, 0.045	1.591, 0.015	0.030, 0.014	247.264, 0.014
IENF density	−0.039, 0.365	−0.008, 0.626	−0.015, 0.552	1.836, 0.056	−2.014, 0.006*	−5.115, 0.267	−7.063, 0.015	−0.105, 0.068	−622.574, 0.153
SSR_palm	−0.171, 0.264	−0.100, 0.071	0.089, 0.332	−6.188, 0.075	3.881, 0.176	12.919, 0.451	25.379, 0.020	0.576, 0.005*	2178.996, 0.180
SSR_sole	0.058, 0.713	0.028, 0.638	0.205, 0.026	−6.622, 0.063	6.864, 0.017	35.457, 0.041	35.029, 0.001*	0.593, 0.006*	1244.591, 0.476
Warm threshold_fd	−0.005, 0.745	−0.004, 0.553	0.0001, 0.991	−0257, 0.476	0.491, 0.093	2.885, 0.093	1.198, 0.297	0.038, 0.085	190.019, 0.255
Cold threshold_fd	−0.004, 0.495	0.002, 0.538	−0.001, 0.747	0.170, 0.253	−0.119, 0.348	−1.363, 0.057	−1.317, 0.004 *	−0.024, 0.008*	−32.629, 0.645
NCS + 5	0.012, 0.586	0.005, 0.489	0.013, 0.310	−0.430, 0.345	0.686, 0.074	5.003, 0.028	3.694, 0.009	0.089, <0.001 *	94.407, 0.667

fd, foot dorsum; IENF, intraepidermal nerve fiber; NCS, nerve conduction study; PND,polyneuropathy disability; R-ODS, Rasch-built overall disability scale; SAS, survey of autonomic symptoms; SSR, sympathetic skin response; WHOQOL-BREF, world health organization quality of life instruments.
*p values passing the threshold of false discovery rate (FDR) < 0.05.

IVSd, and nearly 88% of our patients were associated with an IVSd thickness more than two standard deviations above the mean based on the normal reference. In contrast, only 28.6% of patients showed abnormally low LVEF, suggesting restrictive and infiltrative patterns of cardiomyopathy in our patients. Recent advances in CMR provide a tool to accurately assess the characterization of cardiac tissue and morphology. Cardiac amyloidosis is typically associated with ventricular subendocardial and/or transmural late gadolinium enhancement, increased native myocardial longitudinal relaxation time, increased extracellular volume, and increased LV mass on CMR, reflecting the myocardial amyloid burden.[8,9,37] In the present study, late gadolinium enhancement resulting from the passive distribution of gadolinium in the expanded extracellular space created by amyloid fibrils was noted in 80% of patients. Other CMR parameters, such as myocardial native T1, ECV, LVMi, and MVR, all showed a significant increase in the ATTRv-PN patients compared to healthy controls and age- and gender-matched patients with Brugada syndrome in whom the structures of the heart are normal, indicating the abnormal amyloid deposition in the heart of our patients. These cardiac structural changes due to TTRv amyloidosis were also associated with elevated pro-BNP, a serological marker of heart failure, and approximately 46% of our patients had pro-BNP higher than the normal cutoff value.

In addition to reflecting the morphological and biological characteristics of cardiac amyloidosis, the CMR parameters were also highly correlated with pathophysiological changes of polyneuropathy in late-onset ATTRv-PN, including ECV for cutaneous small-fiber nerve pathology; LVMi and MVR for sudomotor function and the thermal threshold at feet; and MVR for larger-fiber nerve electrophysiology. These findings indicated that the cardiac amyloid burden shown by CMR corresponded to the progression of peripheral nerve degeneration. Due to the close relationship between TTRv amyloid deposition and the degeneration of peripheral nerves,[17,38] the correlation between parameters of cardiomyopathy and polyneuropathy in our late-onset ATTRv-PN may suggest parallel TTRv amyloidogenesis in the heart and peripheral nerves. Furthermore, the CMR parameters were also associated with the functional status of polyneuropathy assessed by PND stage and R-ODS, quality of life measured by WHOQOL_BREF, and autonomic dysfunction evaluated by SAS. These observations supported not only that the severity of cardiomyopathy can reflect the dysfunction of polyneuropathy but also that the involvement of the heart by TTRv amyloidosis contributed to the clinical disability and impaired quality of life. Taken together, the cardiac amyloid burden demonstrated by CMR could serve as a surrogate marker for the degeneration and dysfunction of peripheral nerves in patients with late-onset ATTRv-PN.

There were several limitations in the present study. First, the enrolled patients were from the same ethnic group, and nearly all carried the p. A117S mutation with the phenotype of late-onset ATTRv-PN. The same ethnicity, genotype, and phenotype in the present study may restrict the generalization of the conclusions to all TTRv amyloidosis. Second, this study was a cross-sectional observational study and could not show the temporal changes in the studied parameters. Further prospective longitudinal studies of both polyneuropathy and cardiomyopathy will provide a more comprehensive picture of the association between amyloidogenesis of the heart

and peripheral nerves. Third, the uneven distributions of age and sex between healthy controls and late-onset ATTRv-PN patients might confound the comparison of cardiac parameters between them, although age and sex were corrected as covariates in all statistical analyses.

In conclusion, our observations-based concomitant survey of polyneuropathy and cardiomyopathy suggested that patients with late-onset ATTRv-PN and predominant p. A117S mutation invariably manifested cardiomyopathy regardless of the clinical severity of polyneuropathy. The cardiac TTRv amyloid burden illustrated by CMR was correlated with the pathophysiology of both small-fiber sensory-autonomic and large-fiber myelinated nerves, reflecting the overall disability and quality of life related to simultaneous polyneuropathy and cardiomyopathy and served as biomarkers for long-term follow-up in late-onset ATTRv-PN.

Acknowledgment

The authors thank all the patients and healthy controls for their participation in this study.

Conflicts of Interest

The authors declared that they have no conflict of interest to disclose.

Author Contributions

Yen-Hung Lin, Hsueh-Wen Hsueh, Mao-Yuan Su and Mei-Fang Cheng drafted manuscript, and contributed to acquisition and analysis of data. Ming-Chang Chiang and Jyh-Ming Jimmy Juang contributed to analysis of data, and revision of the manuscript. Yi-Hui Kao, Kai-Chieh Chang, and Fang-Ping Feng contributed to acquisition of data. Sung-Tsang Hsieh contributed to study conception, design and funding, acquisition of data, and revision of the manuscript. Chi-Chao Chao was responsible for study conception, design, funding and supervision, acquisition and analysis of data, and drafting of the manuscript.

References

1. Adams D, Koike H, Slama M, Coelho T. Hereditary transthyretin amyloidosis: a model of medical progress for a fatal disease. Nat Rev Neurol. 2019;15(7):387-404.
2. Mazzeo A, Russo M, Di Bella G, et al. Transthyretin-related familial amyloid polyneuropathy (TTR-FAP): a single-center experience in Sicily, an Italian endemic area. J Neuromuscul Dis. 2015;2(s2):S39-S48.
3. Tozza S, Severi D, Spina E, et al. The neuropathy in hereditary transthyretin amyloidosis: a narrative review. J Peripher Nerv Syst. 2021;26(2):155-159.
4. Koike H, Tanaka F, Hashimoto R, et al. Natural history of transthyretin Val30Met familial amyloid polyneuropathy: analysis of late-onset cases from non-endemic areas. J Neurol Neurosurg Psychiatry. 2012;83(2):152-158.
5. Ruberg FL, Berk JL. Transthyretin (TTR) cardiac amyloidosis. Circulation. 2012;126(10):1286-1300.
6. Koike H, Okumura T, Murohara T, Katsuno M. Multidisciplinary approaches for transthyretin amyloidosis. Cardiol Ther. 2021;10(2):289-311.
7. Lane T, Fontana M, Martinez-Naharro A, et al. Natural history, quality of life, and outcome in cardiac transthyretin amyloidosis. Circulation. 2019;140(1):16-26.
8. Razvi Y, Patel RK, Fontana M, Gillmore JD. Cardiac amyloidosis: a review of current imaging techniques. Front Cardiovasc Med. 2021;8:751293.
9. Martinez-Naharro A, Treibel TA, Abdel-Gadir A, et al. Magnetic resonance in transthyretin cardiac amyloidosis. J Am Coll Cardiol. 2017;70(4):466-477.
10. Martinez-Naharro A, Baksi AJ, Hawkins PN, Fontana M. Diagnostic imaging of cardiac amyloidosis. Nat Rev Cardiol. 2020;17(7):413-426.
11. Huang YH, Lin YH, Yen RF, et al. 2021 advocacy statements for the role of (99m)Tc-pyrophosphate scintigraphy in the diagnosis of transthyretin cardiac amyloidosis: a report of the Taiwan Society of Cardiology and the Society of Nuclear Medicine of the Republic of China. Acta Cardiol Sin. 2021;37(3):221-231.
12. Perugini E, Guidalotti PL, Salvi F, et al. Noninvasive etiologic diagnosis of cardiac amyloidosis using 99mTc-3,3-diphosphono-1,2-propanodicarboxylic acid scintigraphy. J Am Coll Cardiol. 2005;46(6):1076-1084.
13. Plante-Bordeneuve V, Said G. Familial amyloid polyneuropathy. Lancet Neurol. 2011;10(12):1086-1097.
14. Du K, Li F, Wang H, et al. Hereditary transthyretin amyloidosis in mainland China: a unicentric retrospective study. Ann Clin Transl Neurol. 2021;8(4):831-841.
15. Low SC, Tan CY, Md Sari NA, et al. Ala97Ser mutation is common among ethnic Chinese Malaysians with transthyretin familial amyloid polyneuropathy. Amyloid. 2019;26(suppl 1):7-8.
16. Pasutharnchat N, Taychargumpoo C, Vorasettakarnkij Y, Amornvit J. Ala97Ser transthyretin amyloidosis-associated polyneuropathy, clinical and neurophysiological profiles in a Thai cohort. BMC Neurol. 2021;21(1):206.
17. Chao CC, Hsueh HW, Kan HW, et al. Skin nerve pathology: biomarkers of premanifest and manifest amyloid neuropathy. Ann Neurol. 2019;85(4):560-573.
18. Hsueh HW, Chao CC, Chang K, et al. Unique phenotypes with corresponding pathology in late-onset hereditary transthyretin amyloidosis of A97S vs V30M. Front Aging Neurosci. 2022;13:786322.
19. Chao HC, Liao YC, Liu YT, et al. Clinical and genetic profiles of hereditary transthyretin amyloidosis in Taiwan. Ann Clin Transl Neurol. 2019;6(5):913-922.

20. Chien HF, Tseng TJ, Lin WM, et al. Quantitative pathology of cutaneous nerve terminal degeneration in the human skin. Acta Neuropathol. 2001;102(5):455-461.
21. Kahn R. Proceedings of a consensus development conference on standardized measures in diabetic neuropathy. Electrodiagnostic measures. Diabetes Care. 1992;15(8):1087-1091.
22. Chao CC, Tsai LK, Chiou YH, et al. Peripheral nerve disease in SARS: report of a case. Neurology. 2003;61 (12):1820-1821.
23. Chiang MC, Yeh TY, Sung JY, et al. Early changes of nerve integrity in preclinical carriers of hereditary transthyretin Ala117Ser amyloidosis with polyneuropathy. Eur J Neurol. 2021;28(3):982-991.
24. Lin YH, Hsieh SC, Chao CC, Chang YC, Hsieh ST. Influence of aging on thermal and vibratory thresholds of quantitative sensory testing. J Peripher Nerv Syst. 2005;10 (3):269-281.
25. Ravits JM. AAEM minimonograph #48: autonomic nervous system testing. Muscle Nerve. 1997;20(8):919-937.
26. Jerosch-Herold M, Sheridan DC, Kushner JD, et al. Cardiac magnetic resonance imaging of myocardial contrast uptake and blood flow in patients affected with idiopathic or familial dilated cardiomyopathy. Am J Physiol Heart Circ Physiol. 2008;295(3):H1234-H1242.
27. Dorbala S, Ando Y, Bokhari S, et al. ASNC/AHA/ASE/ EANM/HFSA/ISA/SCMR/SNMMI expert consensus recommendations for multimodality imaging in cardiac amyloidosis: part 1 of 2-evidence base and standardized methods of imaging. Circ Cardiovasc Imaging. 2021;14(7): e000029.
28. Knight DS, Zumbo G, Barcella W, et al. Cardiac structural and functional consequences of amyloid deposition by cardiac magnetic resonance and echocardiography and their prognostic roles. JACC Cardiovasc Imaging. 2019;12 (5):823-833.
29. Wu CK, Lee JK, Hsu JC, et al. Myocardial adipose deposition and the development of heart failure with preserved ejection fraction. Eur J Heart Fail. 2020;22 (3):445-454.
30. Bokhari S, Castano A, Pozniakoff T, Deslisle S, Latif F, Maurer MS. (99m)Tc-pyrophosphate scintigraphy for differentiating light-chain cardiac amyloidosis from the transthyretin-related familial and senile cardiac amyloidoses. Circ Cardiovasc Imaging. 2013;6(2):195-201.
31. Dorbala S, Ando Y, Bokhari S, et al. Addendum to ASNC/ AHA/ASE/EANM/HFSA/ISA/SCMR/SNMMI expert consensus recommendations for multimodality imaging in cardiac amyloidosis: part 1 of 2-evidence base and standardized methods of imaging. J Nucl Cardiol. 2021;28(4):1769-1774.
32. Lang RM, Bierig M, Devereux RB, et al. Recommendations for chamber quantification: a report from the American Society of Echocardiography's guidelines and standards committee and the chamber quantification writing group, developed in conjunction with the European Association of Echocardiography, a branch of the European Society of Cardiology. J Am Soc Echocardiogr. 2005;18(12):1440-1463.
33. Chang SN, Sung KT, Huang WH, et al. Sex, racial differences and healthy aging in normative reference ranges on diastolic function in ethnic Asians: 2016 ASE guideline revisited. J Formos Med Assoc. 2021;120 (12):2160-2175.
34. Benjamini Y, Hochberg Y. Controlling the false discovery rate - a practical and powerful approach to multiple testing. J R Stat Soc B. 1995;57(1):289-300.
35. Sekijima Y. Transthyretin (ATTR) amyloidosis: clinical spectrum, molecular pathogenesis and disease-modifying treatments. J Neurol Neurosurg Psychiatry. 2015;86 (9):1036-1043.
36. Gillmore JD, Maurer MS, Falk RH, et al. Nonbiopsy diagnosis of cardiac transthyretin amyloidosis. Circulation. 2016;133(24):2404-2412.
37. Fontana M, Martinez-Naharro A, Chacko L, et al. Reduction in CMR derived extracellular volume with Patisiran indicates cardiac amyloid regression. JACC Cardiovasc Imaging. 2021;14(1):189-199.
38. Fujitake J, Mizuta H, Fujii H, et al. Late-onset familial amyloid polyneuropathy: an autopsy study of two Japanese brothers. Amyloid. 2003;10(3):198-205.

